Metal-as-insulation HTS coils

Thibault Lécrevisse, Xavier Chaud, Philippe Fazilleau, Clément Genot, Jung-Bin Song

Metal-as-Insulation HTS coils

Metal-as-Insulation HTS coils

Thibault Lécrevisse, Xavier Chaud, Philippe Fazilleau, Clément Genot, Jung-bin Song

I. Synopsis:

In this article, we summarize what we have learned about Metal-as-Insulation (MI) winding behavior and technical challenges. Bailey *et al.* first proposed the use of Metallic Insulation (MI) for superconducting magnet in 1988 through a U.S. patent [1]. High Temperature Superconductor (HTS) materials are highly thermally stable. This feature compared to classical Low Temperature Superconductor (LTS) enables the use of MI technology to improve the protection against quenches. Gupta was the first to propose the use of a metallic tape in an HTS winding to avoid too much radial current in No Insulation (NI) in 2011 [2]. Hahn *et al.* presented preliminary results on a pancake sample the same year [3]. We will firstly present a review of the done worldwide since 2011. We will also give details of our LNCMI-CEA-Néel Institute MI HTS insert built in 2018 in the framework of the French National Research Agency (ANR) funding through the NOUGAT project [4]. We tested this magnet many times between 2018 and 2021, firstly under limited background field up to 8 T and then with higher background up to 19 T. The main purposes were to perform tests gradually with increasing the risk, in order to get as much as possible information about UHF (Ultra High Field) REBCO magnets and about the fault behavior of MI magnets. This magnet is the first REBCO solenoid of this size using this technology and tested intensively at such high magnetic field (up to 32.5 T) so far. We are hoping that our experience will help the Ultra High Field (UHF) magnet community to evaluate and adapt the technology to the today and future needs.

II. Introduction

The HTS materials and mainly REBCO (RE is stand for Rare Earth) material are very interesting for UHF magnets or High Temperature magnets. Indeed, they present a much wider potential use than their LTS counterparts (higher magnet field, higher temperature and much higher thermal stability). Their strength – the very high thermal stability due to their high temperature margin - is also leading to their major drawback: the protection against quenches. This issue is mainly due to the very slow longitudinal quench velocity leading to a very high local hot spot temperature. An example of this issue is well described in J. van Nugteren's Thesis [5]. A very interesting solution is to use the HTS high thermal stability, which allows to remove the insulation between turns in a coil without any risks of premature quenches. This solution has been widely studied for about ten years [6, 7, 8, 9]. If many acronyms are presented by research groups around the world (No-Insulation-NI-, Metal as Insulation –MI-, Metal Cladding Insulation –MCI-, Partial insulation- PI-, Smart Insulation-SI-…), all the works are based on the same idea proposed in 1988 by Bailey *et al.* [1]. By removing the insulation between turns, we allow the current to bypass a local quenched part in an HTS winding and avoid a local burning. This solution is highly simplifying the coil fabrication and magnet operation. We can also simplify the protection scheme, which might be very challenging and costly in a high field HTS magnet [10].

In this article, we highlight the operating condition of MI coils without coming back on the modelling or already highlighted specificities. Most elements (like advantages or drawbacks) have already been widely explained otherwise, see e.g. Hahn's 2018 article [11]. The very high thermal stability, the self-protection against local transition and the mechanical robustness are three of the major advantages of such windings. The major drawback of NI technology is the transfer of the overheating (quench) issue of insulated coils to a mechanical issue due to new unbalanced and torque forces. Such new

forces repartition results from the generated radial currents. The complexity of the NI (or MI) electrical circuit compared to their insulated counterpart requires thinking again the way to study the behavior of a mockup and to validate the models. In another words, if the mockups and experiments are much simpler to perform, the analyzing of the data is however more complicated. We need a reliable numerical model based on complex codes in order to evaluate and extrapolate the behavior of a MI coil in particular conditions (quenches, charging or discharging operation…). In addition, the simulation time (related to the model complexity) requires a huge work of coding in order to model a full magnet and perform the simulation in a reasonable time. Such developments are necessary for the understanding of the magnet behavior during transient events and for the winding optimization. For now, the today models and coding do not allow such optimization.

In order to highlight some specific aspects, we will propose the analysis of new data from our MI magnet: the NOUGAT insert for which we already published the main result without detail analysis of the data [12]. We also widely studied the behavior (including the resistance to quenches at high field) on a two-DPs prototype made of THEVA and SuperPower tapes [13]. We will not come back on this magnet results in this paper. We will also detail a specificity of the two magnets which is the magnetic shielding consisting of HTS NI turns inside the overbanding. We only understood recently the real effect of such shielding during the fast transients of the magnets. We tested both magnets intensively and performed several quenches under high background field and high current. From our experience, which is quite consistent with numerical and experimental works performed by Kasumata *et al.* [14], Lu *et al.* [15], Sohn *et al.* [16], and Bonura *et al.* [17], we consider that the most important parameter in the development of the MI technology is the turn-to-turn contact resistivity, R_{ct}.

In a first part, we will present and discuss the Turn-to-turn contact resistivity values obtained by few groups worldwide, depending on the technological choices and the way chosen for estimating R_{ct}. As we will show, the values are highly related to the way they are measured and it is an even more critical aspect as the R_{ct} is going huge. We will highlight the uncertainty we might have on the measured values, considering firstly the measurement on a stack and then a numerical approach using our newly developed PEEC model. In the second part, we will focus on our NOUGAT magnet, which is giving some very interesting results on the good protection against local hotspots or outsert major events. We will introduce here the specificities of our magnet, which include a Magnetic Shielding (MS). J.C. Vallier proposed this concept in 1996 [18]. The role is to shield (or at least 'smooth') every variation of external magnetic flux; this is a well-known technology used in hybrid magnets [19] [20]. In our magnet, the MS consists of REBCO NI turns implemented in the middle of the Stainless Steel (SS) overbanding (OB). An and Mato [21] [22] have numerically shown in 2020 and 2021 the beneficial effect of such technology in the peak temperature and stresses during quenches of an NI magnet. We can confirm it with our magnet built in 2018, which handled a sudden discharge of the outsert (and of itself) at very high field (above 28 T), and a quench at 32.5 T, without mechanical breaking of the winding. Finally, we will discuss of what seems important to us: how the MI technology might help to protect HTS magnets, and how we can optimize it depending on the application. We are looking at a behavior as close as possible to an insulated magnet but with a protectable magnet.

III. The Metal-as-Insulation (MI) winding

At the start of the NOUGAT project in 2015 aiming at the fabrication of a 10 T HTS insert to operate in a 20 T background field. The first idea of using stainless steel between turns was to improve the mechanics in an HTS coil [2] [6]. At this time, researcher did not consider the co-winding of stainless steel to increase the resistance between turns. Only a few articles presented this possibility and without details on the impact [3], [8]. We considered two options at the beginning of the project: the MI solution and the alternative, the most common insulated one. However, after looking at what we

might do as a design in the very limited space we had, we estimated that the protection of our insert using the classical insulated approach would be impossible. We started to look at innovative winding solutions on small pancake coils (NI and MI) and we concluded that the NI technology was not suitable for our project: it introduces too much uncertainty on the contact resistance value and on the mechanical behavior of the coil during a quench. In [23], Markiewicz et al. performed a parametric study on the electrical quench propagation in NI-MI coils depending on the R_{ct} value. The main results are very interesting and helpful. Markiewicz et al. gave a wide range of R_{ct} for which the quench propagation between sub-elements is working well (self-protection behavior). In addition, the mechanical transient unbalanced stresses are reduced in a significant way when increasing the turn-to-turn contact resistivity. This confirm the advantages of increasing the turn-to-turn contact resistivity, and at posteriori, the choices we made for our magnet. The other drawback was a very large time constant not compatible with our expectancies to propose a magnet to users. We started to work on this technology in 2015 with a first approach of looking at quench behavior within a small pancake cooled down at 77 K (LN2) [24]. Another similar work has been done at 77 K (LN2 or conduction cooled) by Sohn *et al.* [25]. Both studies confirmed that such windings are highly thermally stable against local heat dissipation and might handle a quench at high current without local thermal damages.

We decided to generate quenches within a highly instrumented MI REBCO pancake [26] and then to test the technology on a two double pancake magnet [4]. All those prototypes highlighted two major facts: the technology decreases the time constant of the magnet and show a very good efficiency to protect UHF magnets with a simple electrical circuit. We will detail later our protection scheme. This solution is now widely studied for HTS magnets and recent work from Lu *et al.* [15] highlighted the role of the tape surface oxidation, the effect of cooling, and the mechanical cycles in the high R_{ct} obtained and its fluctuation. According to Lu *et al.* work, the oxidation layer is creating a very thin and weak, but highly resistive layer. Such layer is increasing the turn-to-turn contact resistivity. In most case, this layer is created during storage and coil fabrication, leading to an unpredictable resistance, which is fluctuating significantly during the magnet lifetime. This fluctuation aspect is a major technological challenge, as we need a predictable magnet behavior. We have to understand what is modifying the R_{ct} (and so the transient behavior) and if the change is affecting significantly the magnet behavior. The advantages of MI technology compared to the NI counterpart is that an important relative fluctuation of the contact resistance R_{ct} might have a low impact on the magnet behavior. Indeed, the very high original value might be decreased by a factor two without significant impact on the transient behavior. We will come back on this aspect with measurements of the time constants of the NOUGAT insert along the many tests performed at 15 T and above.

IV. The contact resistivity: a key parameter for transient behavior

The contact resistivity between turns in NI or MI magnets is a major parameter, which is driving the magnet transient behavior and the magnet self-protection feature. We are able to evaluate the transient magnet behavior through numerical modelling if we precisely know the contact resistivity - R_{ct}- value and if this value is not changing significantly because of local parameters – like mechanical pressure between turns for instance - and along the magnet lifetime. Table 1 summarizes values of the contact resistivity obtained by a few groups depending on the technology and experimental setup.

As already highlighted by Lu *et al.* [15], the surface oxidation plays an important role in the R_{ct} values of NI or MI windings. A simple estimation of the material part on the global R_{ct} value shows that the thickness and material have a contribution of about 0.06 μΩ.cm² (Hastelloy® with: $\rho_{Hast} = 1.23\ \mu\Omega.m, t = 50\ \mu m$). This contribution is insignificant when looking at the 100 to 10000 μΩ.cm² for MI winding reported in Table 1. When looking at what is influencing the R_{ct}, we can identify the surface quality (roughness, thickness fluctuation and oxidation), the hardness of the material, but also

experimental parameters like the mechanical pressure [15] [16] [17]. It is now evident that many materials or experimental aspects, which were not pinpointed at once during the R_{ct} measurements reported in Table 1, are influencing the R_{ct} value. Therefore, all numbers in the table have to be considered carefully.

Another aspect to consider when looking at the R_{ct} from experimental point of view are the measurements methods. Two ways are possible: measurement within a coil and measurement within a stack sample. The first one is much more complicated to analyze. Indeed, the lowest the R_{ct} is, the highest the radial currents are. It leads to a mismatch of the experimental R_{ct} obtained from the field decay and the theoretical R_{ct} obtained from a numerical model (like a PEEC model). If looking at the very high R_{ct} value, the time constant might be very low (order of several milliseconds) and the acquisition rate should be able to go beyond 5-10 kHz to have enough acquisition data during the discharge. This behavior is also highlighted by Mun *et al.* [27]. In this reference, the time constant was not measurable (below 0.22 s) due to the limited acquisition frequency. The acquisition set-up details to obtain the data reported in Table 1 do not allow checking the accuracy of the R_{ct} value. In Figure 1 we are considering a MI coil discharge obtained from our Partial Equivalent Electrical Circuit (PEEC) model [9]. The principle of the PEEC model is to divide each turn of a pancake into several identical angular sectors. Each created sector is defined by a variable longitudinal resistance R_θ (superconducting or not) and an inductance $M_{k|i}$ as presented in Figure 2. The radial resistance between two radially adjacent sectors R_r is estimated from the R_{ct} parameter (we gave the details of the model in [28]). We implemented the critical current fit from J. Fleiter [29]. The results are fitted with an exponential decay model done classically for the estimation of R_{ct}. We consider a four pancakes magnet with 200 turns per pancake. The inner diameter is 50 mm and each turn consists of a 72 µm thick HTS tape, 6 mm wide, co-wound with a 50 µm thick stainless steel tape. The R_{ct} value is set at 10 mΩ.cm². With those considerations, the estimation of the R_{ct} from the central field Bz_0 decay is 9.45 mΩ.cm², which is about 5.5 % lower than the model parameter value. Most of the windings R_{ct} evaluations are made using such magnetic field decay measurements on small coils. As explained above, it might lead to an inaccurate R_{ct} value. An alternative way would be to estimate the R_{ct} value through a numerical model in representative mockups (small enough to be accurately simulated in a reasonable time scale).

The measurement within a stack seems therefore more reliable to evaluate the intrinsic turn-to-turn contact resistivity without adding the experimental bias of measurements on a coil.

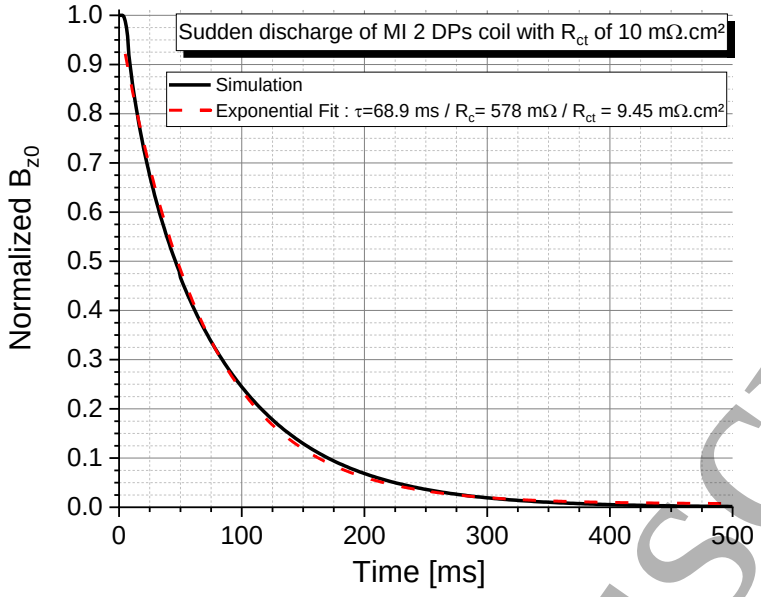

Figure 1: Sudden discharge of an MI magnet at 10 A obtained from PEEC model

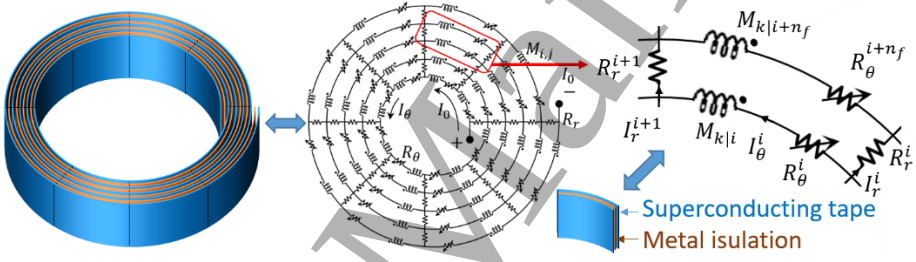

Figure 2: PEEC network scheme from [28]

Table 1: Overview of the R_{ct} published values for NI and MI windings

Technology	Sample type	Temperature	R_{ct} ($\mu\Omega.cm^2$)	Ref.
NI	Small pancakes	77 K	70.7-71.3	[7]
NI Thermal Grease insulation (TG)	Small pancakes	77 K	NI:15.2 TG : 23.1 *	[30]
NI	Small coil		12.8	[31]
NI MI Brass	Small pancake	77 K	25.5 46.8	[32]
NI	**Stack 2 tapes 25*4 mm²**	**77 K**	**26-100**	[33]
NI	Small pancake	77 K	48.3-56.8	[34]
MI Stainless Steel (SuS) MI Copper	Small pancakes	77 K	155 60	[8]
NI MI SuS 304L	Small pancake	77 K	19.2 1100-9800	[24]
MCI	2 DPs magnet	4.2 K	130-280	[35]
MI Durnomag®	2 DP magnet	4.2 K	207	[4]
MI Durnomag®	Single pancake	4.2 K	615-810	[26]

MI Durnomag®	Double pancakes and magnet	4.2 K	1000	[13]
NI SuperOx	Small pancake		29.2-33.2	[36]
NI (oxide removal) **MI SuS 316** **MI CuZn37**	**Stack 2 tapes 12*4 mm²**	**77 K**	**80-100 (2-3)** **3000-4000** **120-900**	[17]
MI SuS MI SuS pre-tined MI SuS soldered	Small pancakes	77 K	> 293 292.7 25.5	[27]
	* : estimated from the resistances and coils geometry in the paper			

In order to give a feedback of the MI experience we performed, we present in Figure 3 the sudden discharge measurement of five DPs of our insert. We obtained the discharge by opening a mechanical breaker without a dump resistor connected to the coil. As the measurements in 2018 were our first measurements on significant MI DP, the results are not satisfactory due to low acquisition frequency. After the successful tests in 2019, we repaired the inner joints of each DPs and the Bz0 data (magnetic field at the center of the double pancake) shown in Figure 3 are the "refurbished" DPs charged at 20 A before the sudden discharge. We repeated the discharge three times to check the reproducibility; we present here the second discharge for each DP. We used a 10 kHz acquisition NI c-DAQ. From the exponential fits performed on the first 70 ms, we obtain a time constant between 2.3 ms and 6 ms for the nine DPs. Considering an inductance of 26.46 mH we might estimate the R_{ct} between 0.11 and 0.29 Ω.cm². This estimation considers a constant R_{ct} along the winding and is obtained from equation (1), where R_c is the total contact resistance of the coil and S_i is the i-turn average contact surface. We present experimental field decay curves and exponential decay fits in Figure 3 left for the first 35 milliseconds of the discharge. The exponential decay fit does not reproduce precisely the whole discharge but gives a consistent time constant value from the discharge. On the right chart, we present the same DPs data with our PEEC model results for R_{ct} values of 0.05, 0.10, 0.30 and 1 Ω.cm². From the results, we might estimate the R_{ct} of our MI DP coils between 0.10 and 0.30 Ω.cm². The two approaches give the same range of R_{ct} values. Despite the wide range of R_{ct} values obtained for the nine DPs (about 0.2 Ω.cm² fluctuation), it shows that the chosen solution for the magnet led to high R_{ct} values. In addition, it shows that the transient behavior difference between the DPs is only visible during the first tens of milliseconds (time constant fluctuation of 4 ms between DPs). It is an important aspect to lower the unbalanced forces when operating the magnet or in case of a fast discharge.

$$R_c = R_{ct} * \sum_{i=0}^{N} \frac{1}{S_i} \quad (1)$$

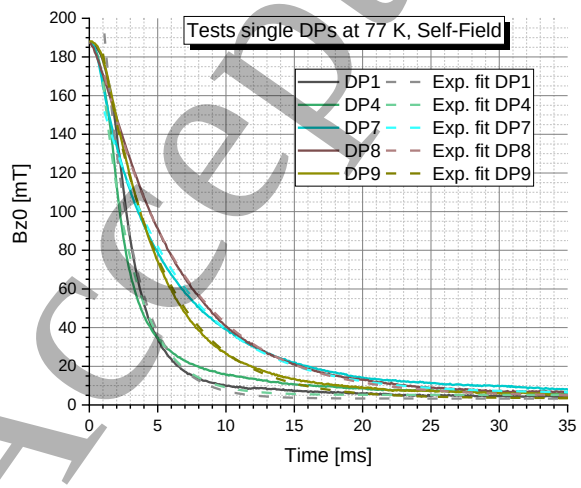

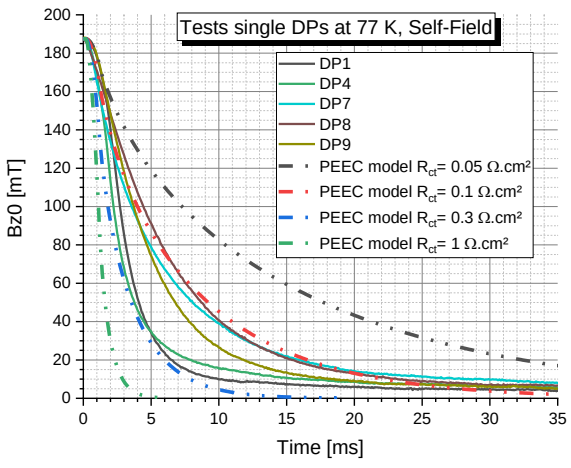

Figure 3: NOUGAT "refurbished" five DP coils 2020 sudden discharge at 20 A: with exponential decay fit (left) and PEEC model with 4 R_{ct} values (right).

A solution to avoid the bias of the measurement set-up would be to study the resistance on a stack. Lu *et al.* and Bonura *et al.* considered this approach for NI and MI solutions [33] and [17]. We also started a study at CEA on a similar configuration but on a 290*6 mm² sample area at 77 K (LN_2). We present a CAD model of the experimental setup and a picture in Figure 4 and Figure 5 respectively. The superconducting tapes are set in the "U" shaped stainless-steel part. In order to carry out the measurements according to the mechanical stress, another "T" shape part in stainless steel is put on the tapes. The samples are powered using copper current leads (rods). The length of the stack of superconducting tapes is representative of the length of the turns of a coil. We summarize in Figure 6 the main results obtained from voltages measurements using a National Instrument cDAQ system : we evaluated the influence of four the manufacturers (SuperPower©, THEVA,Shanghai Superconductor Technology (SST) and SuperOx), the NI and MI windings and the influence of the mechanical pressure. When comparing the results to the values presented in Table 1, we measured R_{ct} values that are 4 to 7 times (NI) and beyond 10 times (MI) higher than the values reported in [17] and [33]. We measured the R_{ct} values within a long stack (290 mm) compared to the reported values (4 mm and 12 mm). The sample length might have a significant influence on the measured values, because of the thickness fluctuation along the tape length. It is therefore important to have a length representative of a coil turn perimeter. In addition, as it was already stated *supra*, the number of load cycles, as well as the mechanical pressure on the interface highly affect the values. We present some R_{ct} ranges in Table 2 for NI and MI windings with two different metallic tapes: a 304 soft hardened stainless steel, a special extra hard stainless-steel alloy (Durnomag®). As the values depend on the mechanical pressure and load cycles, we give the ranges for a mechanical pressure of 50 MPa and after a few load cycles (not the virgin state during the first cycle). All our samples are using tapes as received (no oxide layer removal). The main results here are the high increase of the contact resistance when inserting a soft stainless-steel tape between turns. An extra hard stainless steel is increasing much more the contact resistance (by about three orders of magnitude compared to NI and a factor two to four when comparing to a soft stainless steel). In the case of SuperPower MI case with Durnomag® (like our NOUGAT magnet), the range is in good agreement with our previous estimation (100-300 mΩ.cm²).

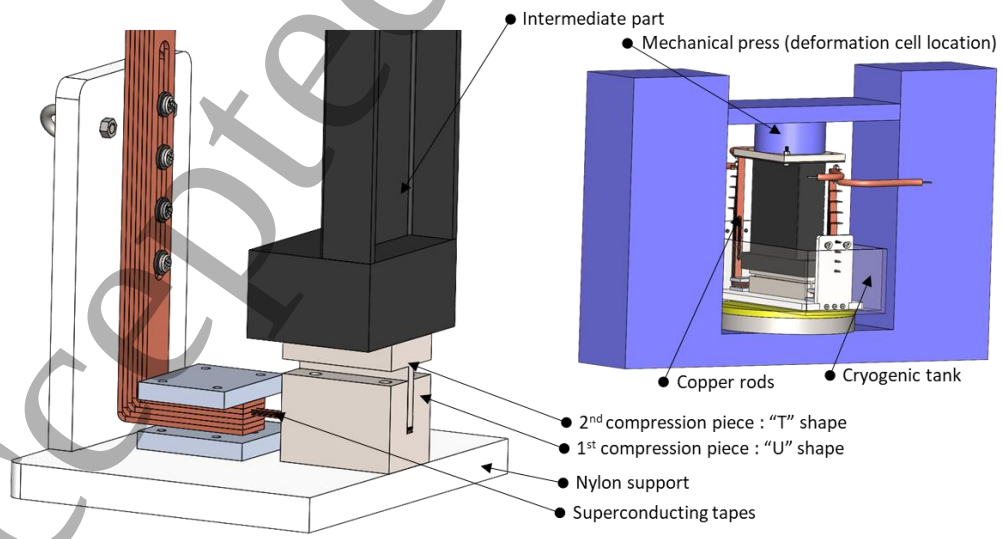

Figure 4: CAD of the stack interface measurement experimental setup

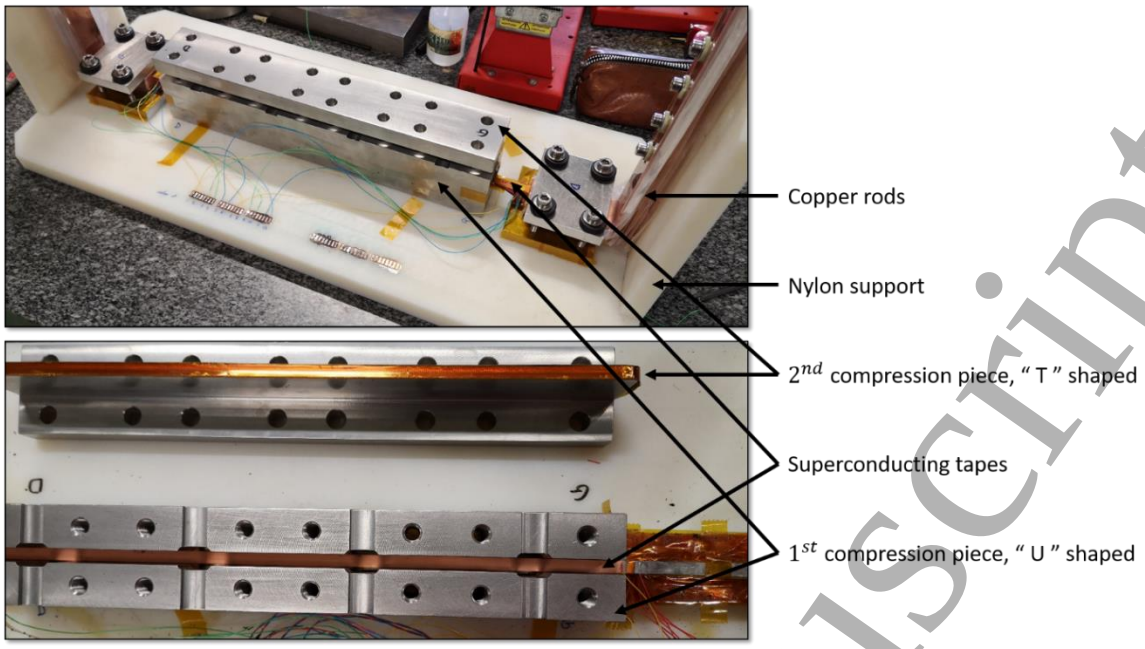

Figure 5 : Experimental setup for contact resistance measurement on stack

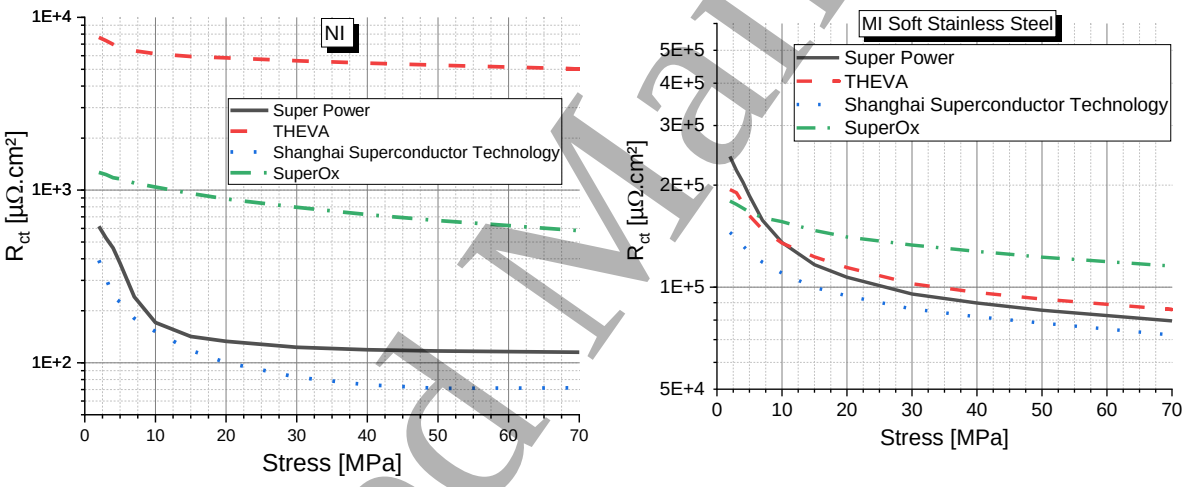

Figure 6: NI (left) and MI (right) R_{ct} values and pressure influence on a 290 x 6 mm² surface

Table 2: R_{ct} values for NI and MI stacks of SP, THEVA, SST and SuperOx HTS tapes at 50 MPa of pressure

R_{ct} [mΩ.cm²]	SuperPower	THEVA	SST	SuperOx
NI	0.12-0.80	4-9.8	0.06-0.08	0.30-0.80
MI Stainless Steel (soft hardening)	71-77	58-112	56-80	80-160
MI Durnomag® (extra Hard)	279-410		280-360	145-230

V. NOUGAT MI Magnet

A. NOUGAT insert and design

In the framework of the ANR project NOUGAT, we decided in 2016 to build the first MI magnet designed to reach 30 T in a 20 T resistive background field. The use of the 20 T resistive magnet in this project was a quick way to confirm that REBCO HTS materials are suitable for producing above 30 T in a user compatible size (38 mm cold bore). We present a scheme of the experimental magnetic configuration and a picture of our NOUGAT insert in Figure 7. Before building the final magnet, we performed some tests on a single pancake [26] showing that such technology might be very efficient for the self-protection feature, in case of a local quench under high field. We also built and tested a two-Double Pancake prototype to reach very high mechanical stresses with sub-elements similar to the NOUGAT DPs [13]. As all those results were very encouraging, we built our insert in 2018 and tested it starting October 2018. We performed the main tests in February and March 2019, including the world record magnetic field of 32.5 T for a 38 mm aperture insert. Before reaching 32.5 T (in a background field of 18 T), we also tried a test under 19 T but the resistive magnet got an issue which led to a slow discharge followed by a fast one around 11 T.

We presented the details of the magnet in our previous publication [12]. For reminder, the magnet consists of 18 pancakes assembled in nine double pancakes with internal joints. The winding diameter is 50 mm (leaving 38 mm aperture) and each pancake is made of 290 turns. Each turn is composed of a 6 mm-wide and 75 µm-thick SCS6050-AP SuperPower REBCO tape (incl. 50 µm of Hastelloy substrate and 20 µm of copper stabilizer) co-wound with a 6 mm-wide and 30 µm-thick Durnomag® tape provided by Lamineries MATTHEY SA. The Durnomag® tape is cold-worked in extra hard state in order to reach very high elastical limit. The magnet is dry wound.

A specificity of this magnet is the presence of a REBCO NI magnetic shielding inside the coils over-banding. For two years, we have been developing the numerical tools to understand the effect of such passive magnetic protection. The principle is similar to the shield used in hybrid magnets [20]. The NI magnetic shielding consists of three 6 mm-wide SCS6050-AP NI turns inserted after 1 mm (13 turns) of over-banding around each pancake. We discuss the magnetic shielding more in details in the following section *G*.

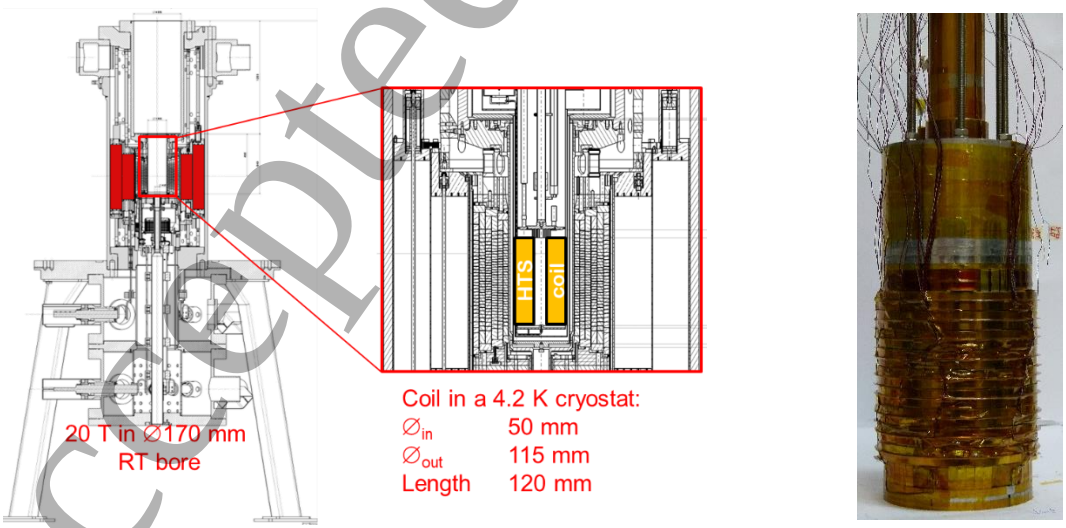

Figure 7: Schematic view of the NOUGAT insert inside the 20 T Resistive magnet at LNCMI-G (left) and picture of the NOUGAT insert (right)

B. Tests of the magnet

After the preliminary developments of small mockups between 2016 and 2018, we fabricated the final insert in 2018. We adapted our tests sequences to the availability of the resistive (Ω) background field installation and started the tests in a background field limited to 8 T in October 2018. As the results were very encouraging, we continued the tests in a background field up to 19 T in February and March 2019. For each sequence, we tried to get as many data as possible including sudden discharge with or without a dump resistor at low current (10 A to 50 A), a test above the nominal current (up to 300 A) at intermediate background field. In addition, to check the signal evolution through the tests, we manage to perform a preliminary test at 150 A and a final test at the same current for each outsert magnetic field value. We will detail in the following section the main measurements of the resistive magnet fault at 19 T and the test where we push the magnet far above its nominal condition up to the thermal runaway at 32.5 T. Those two tests are a good example of how strong such windings are against unpredicted faults, even without a complex protection scheme. Then we will come back to an important aspect, which is the magnet behavior and its stability along the tests.

C. Background field failure at 19 T and effect on the insert

After successfully reaching 30 T in a 12 T (HTS)/ 18 T (Ω) configuration, we decided to increase the background field to test the magnet at its nominal current (225 A corresponding to 10 T) in a 19 T background field. For this test, we charged the insert with a current ramping rate of 0.5 A/s (corresponding to 21-23 mT/s). During the final verification step at 150 A (see Figure 8 left), the resistive magnet security system triggered and activated a slow discharge of the resistive magnet (at 990 s from the start of the test); it induced an increasing current inside the insert by magnetic coupling. At t=1064 s (74 s after the starting of the resistive magnet slow discharge), we manually opened the HTS breaker in order to stop the current increase inside the insert and to prevent any damages. The HTS current and magnetic field dropped nearly to zero in about 2 s. Finally, the fast discharge of the resistive magnet occurred at t = 1109 s. This unexpected event led to damages of the instrumentation and probes. Nevertheless, we still were able to measure the global voltage of the HTS insert and the central magnetic field. Because of the MI “self-protection” feature, we decided to continue the tests under 18 T to prevent any new issue with the resistive magnet.

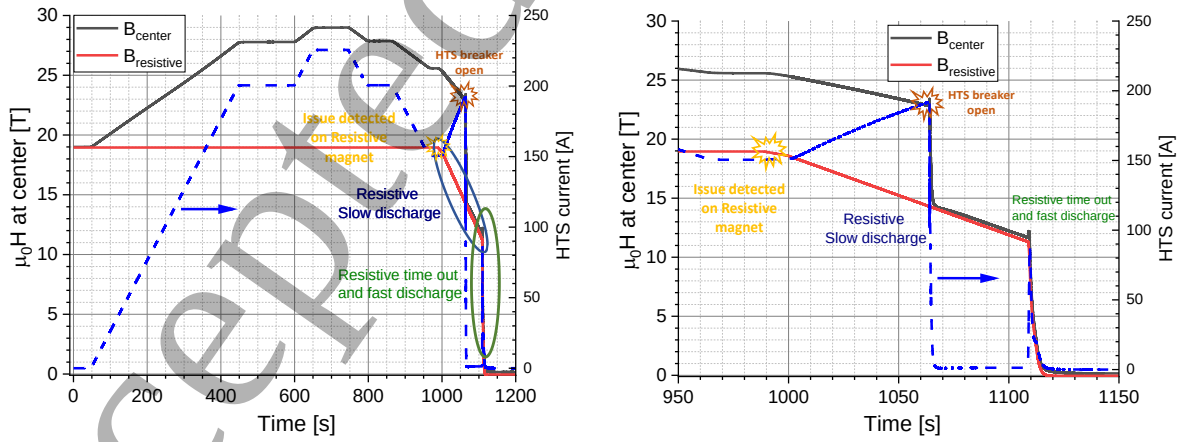

Figure 8: NOUGAT insert test under 19 T background field global view (left) and resistive issue zoom (right)

D. The 32.5 T maximum field and thermal runaway test

After the issue of the resistive magnet at 19 T, we decided to operate the resistive outsert at 18 T and to push the insert above its nominal current/self magnetic field and we observed the behavior beyond this limit. Due to instrumentation damages during the former test, we only were able to measure the

global voltage inside the cryostat (including HTS and resistive current leads). We present the coil current, voltage, central magnetic field and the temperatures (coil bottom and top pancakes) in Figure 9 and Figure 10. During this test we set the Over Voltage Protection (OVP) value of the power supply at 2 V (the HTS coil power supply switches off automatically if the voltage reached the OVP value) and deactivated the protection (discharge inside a dump resistor) related to the voltage threshold. We manually opened the breaker at t = 1246.7 s (~50 s after the start of the quench). During the pre-quench phase (Figure 10), the temperatures increased to 7.5 K and above. The coil voltage slightly increased from 40 mV to 170 mV just before the quench. This voltage is far below the OVP setup voltage and when the quench occurred, the global voltage went negative. As the power supply was only allowing positive current and positive voltage (one quadrant PS), the current passed through the Free Wheel Diode (FWD) of the power supply. During the magnet quench and discharge, a voltage fluctuation above 1.5 V led to the triggering of the PS OVP and the magnet continues to discharge the energy into the cold environment. The HTS energy (about 44.6 kJ) was dissipated inside the liquid helium bath in about 900 ms leading to a complete boil off and to an increase of the temperature of the bottom stainless steel plate (bottom temperature sensor) of the magnet to 110 K. During the fast transient, the Cernox top temperature sensor was damaged and we lost the signal from the probe (black plain line). As we cannot see any two-time-constants discharge of the magnet specific to an external flux variation (cf. section G), we are confident that the NI magnetic shied quenched due to the very high-induced current coming from the HTS magnet quench. It probably helped to avoid a too high-unbalanced stresses inside the magnet.

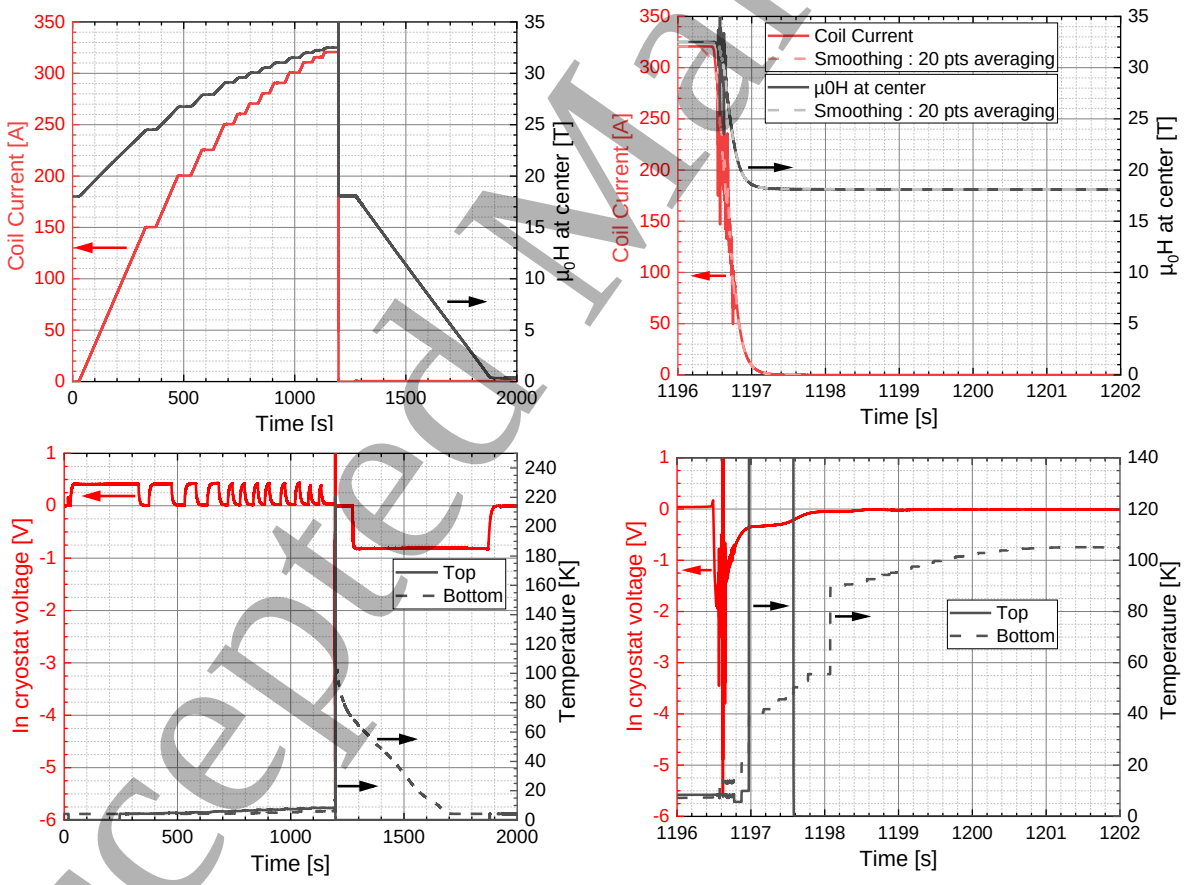

Figure 9: Test under 18 T background Field and quench at 32.5 T - Global (left) and zoom on quench (right)

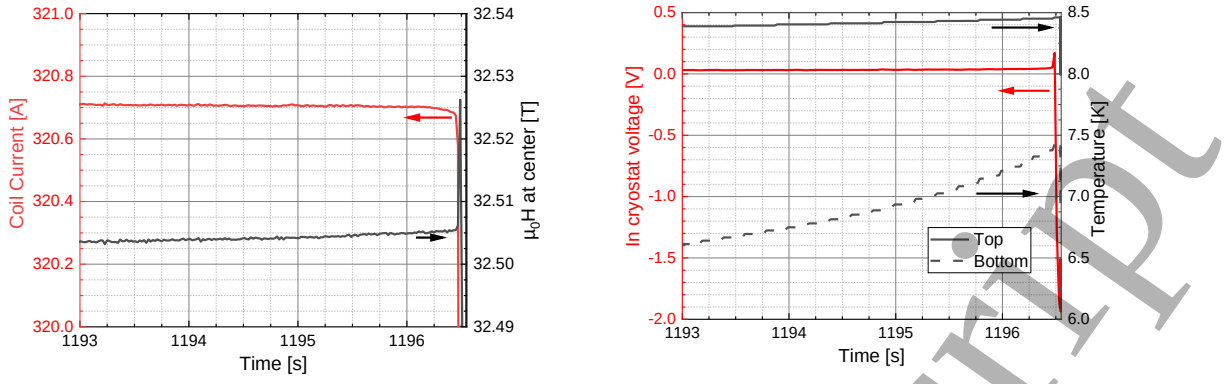

Figure 10: Test under 18 T background field - prequench signals

Following the quench, we checked the magnet status by tests in self-field configuration and we confirmed that the magnetic field generation was identical (in the SCIF fluctuation accuracy range) to the first tests. However, we observed a larger thermal dissipation not compatible with the cooling capacity of the cryostat at 300 A. We stopped the tests and dismantled the magnet in order to evaluate the damages. Despite the very constrained tests and the two major events, the main damages were very localized at the inner and outer joints. After repairing the joints, the magnet behavior is identical to the initial tests (up to 9.5 T background field and 300 A, as the higher field resistive magnet configuration was not available at the time of this article preparation).

E. Time constant evolution along the tests

The time constant of the magnet is a major parameter, which is driving the possibilities of using it in specific user's requirement. This time constant reflects the possibility of fast charge and discharge of the magnetic field and therefore drives the test time for the experiments. In MI coils, the time constant is directly linked to the resistance between turns. A MI magnet can be modeled in a first approximation (with a limited accuracy as explained in section IV) like a pure inductance in parallel to a resistance corresponding to the sum of all the turn-to-turn resistances (called R_c in our paper). If the absolute value is debatable, a fluctuation of the magnet time constant along the tests is directly related to a fluctuation of the R_c. Figure 11 shows the simplified electrical circuit of the MI coil. In order to determine the time constant of the magnet and the average R_{ct}, we performed several discharges without a dump resistor with 10 A inside the magnet in self-field. We estimated the time constant from an exponential decay fit of the discharge.

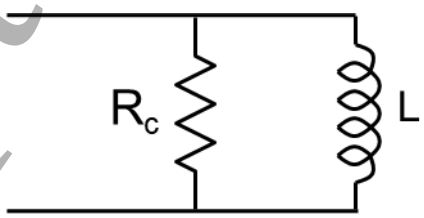

Figure 11: Simplified electrical circuit of the MI magnet

We present some field discharges from tests performed in 2018, 2019 and 2020 in Figure 12. The specificities of the tests are the following:

- Tests 20180919: firsts tests of this magnet (sort of virgin state after the first cooling sequence)

- Tests 20180921: Sudden discharge tests after a test at 300 A in a 8 T Ω-field (meaning after some electromechanical cycles).

- Tests 20190320: Initial tests in 2019 after warming up and storage inside the cryostat for 6 months.

- Tests 20200207: Initial tests in 2020 after Instrumentation and over-banding repair.

- Tests 20200208: Final tests after tests up to 325 A in a 9.2 T Ω-field.

We can identify the two-time-constant specificity on Figure 12 (see section G for explanations about the two-time-constant discharge). The data are sometimes difficult to compare as the initial test magnetic field is including the SCIF and so depends on the previous tests configuration. We aligned all the initial magnetic fields at 0.42 T so that the onsets of the discharge are easier to compare even if the end will highly depend on the part generated by the SCIF. The first element we can extract from this figure is the effect of the magnetic shielding. We can see the two-time-constant due to the magnetic shielding in the top right chart. More than half of the field is discharge after 500 ms. We reproduced all the tests at least two times and the curves of identical tests performed in series are superposed. We can identify a significant change after the first tests at high current under field in 2018.

The time constant (determined on the first 400-500 ms of the discharge) changed after the few first tests of 2018 campaign and then stayed quite constant. The change of behavior in the second part of the discharge after the repair of the instrumentation in 2020 (for which we have to change the OB and the NI magnetic shielding) is not well understood. In order to repair the instrumentation, we have to access to the voltage taps connected before the overbanding. Therefore, the difference might come from the new tapes used for the NI magnetic shielding and/or its realization. An important result here is the efficiency of the magnetic shielding, which help to transfer a part of the stored energy within the NI SC turns. We will discuss about this technology in section G.

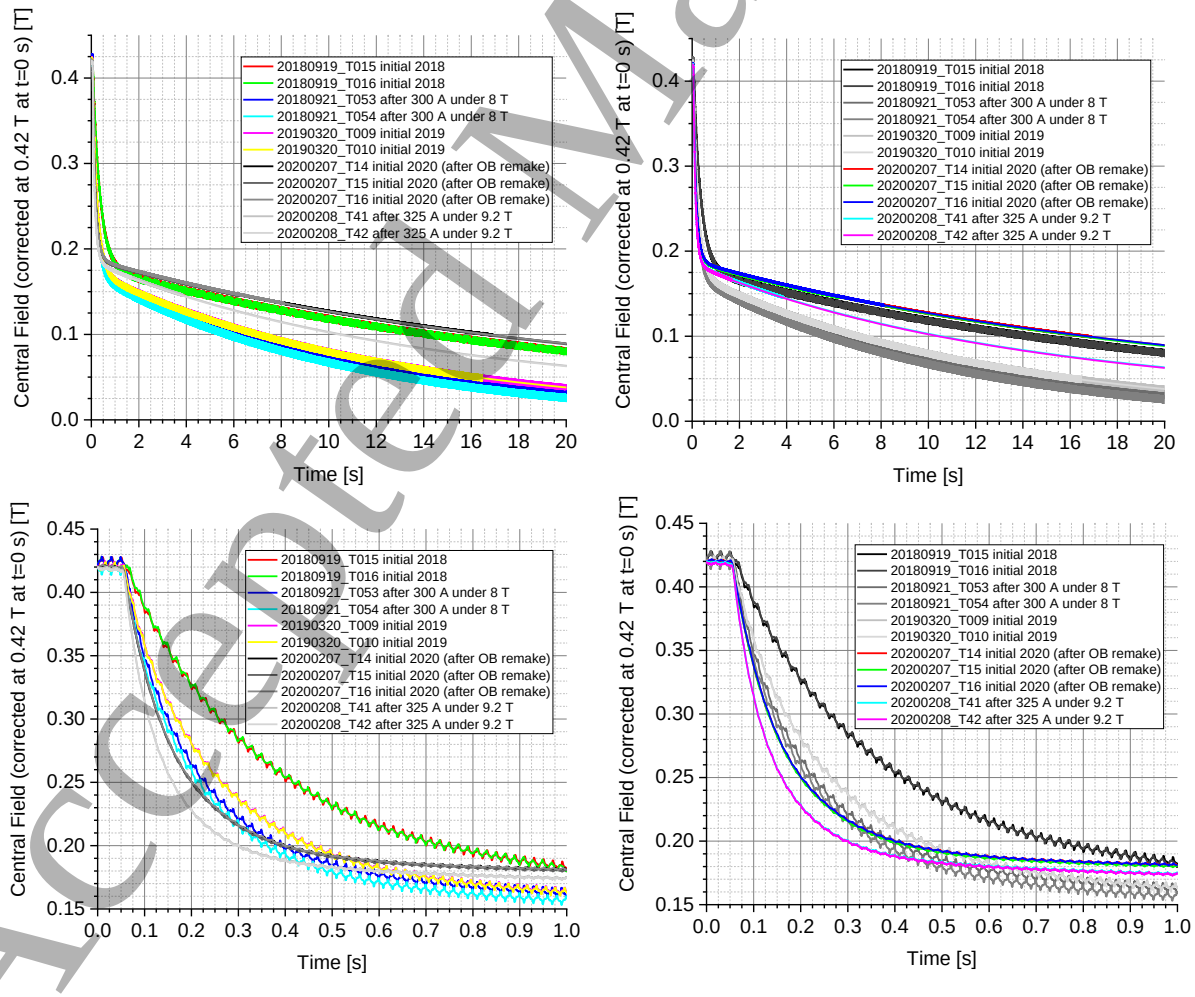

Figure 12: Field Decay in Self-Field with 10 A inside NOUGAT insert

F. Lessons from the NOUGAT insert tests

If we do not fully understand all the results because the numerical models required are still under development for significant magnets, we confirmed many advantages of MI technology:

1- The MI technology is greatly simplifying the protection scheme as the radial currents generates a voltage that is high enough to be easily detected without any risks of local burning. Nevertheless, we do not consider that a winding with a high R_{ct} value, which is required to lower the time constant and the unbalanced stresses, is still self-protected. It is important to detect the transition (in the 100-500 mV range) and to stop the powering of the magnet.

2- With this technology, the tests are easier than with insulated windings (no needs of high speed, low noise acquisition system or dedicated Magnet Safety System – MSS). It enables fast developments on specific aspects under high stresses/fields due to the low risk of damaging sample / mock-ups and simplifies the experimental setup.

3- As the high R_{ct} value is significantly lowering the radial current magnitude, this technology allows faster charging and more accurate magnetic field generation during the charge and the discharge. It is therefore more adapted to applications where the field as to follow specific time profile like for the ultra-high field inserts.

4- If the cooling is sufficient, an MI magnet can work in a stable matter very close to the quench current and without any training.

5- Like NI windings, the generated magnetic field is identical to the insulated counterpart after a delay due to the bypassing radial currents decay. In our experiments, the time constant during charging of the NOUGAT insert under 18 T is closed to five seconds (assuming a 3 τ criteria).

6- All the unexpected events did not significantly damage the magnet. The weakest parts for very high field application are the pancake-to-pancake joints, which are easily delaminated (even without unexpected events). We have to work on the joint technology in order to obtain not only low resistance joints but also joints, which can handle very high mechanical stresses.

7- In case of sub-element damages, the pancakes can be unwound and the tapes reused without seeing a major change in the sub-element and magnet performances.

G. The specificity of the conception: the magnetic shielding

We have shown *supra* that the insert survived to the resistive magnet failure without any impact on the magnet performance. Part of this robustness may be attributed to the MI technology, but the role of the magnetic shielding (MS) is also at stake, especially when looking at outsert fault. We developed numerical codes to study the transients of such magnets and the recent simulations have confirmed the protection feature brought by magnetic shielding. It was already shown for hybrid magnets [20]. The idea consists in inserting a magnetic shield between the HTS winding and the external one (LTS or resistive) in order to reduce the high induced currents and unbalanced stresses during the fast transient of NI-MI or outsert magnets. When building our NOUGAT insert in 2018, we implemented this solution by adding several SC NI turns (three) outside the windings of each pancake, in the middle of the overbanding turns (about 1 mm of SS between the coil and the NI turns and 3 mm of SS after the NI turns). We present a sketch of this solution in Figure 13.The SC turns as a whole act like a complete shield from any external magnetic flux variation.

As stated supra, when discharging the magnet, its current follows a two-time-constant evolution. This is due to the presence of the magnetic shielding. Figure 13 shows a simplified electric circuit of the magnet (R_1, L_1, I_1) and the magnetic shielding (R_2, L_2, I_2). The time evolution of current is easily estimated analytically with Kirchoff's equations and the results are shown in equation (2). I_0 is the current at the beginning of the discharge and we assume the current of the magnetic shielding is null. A, B and C depend on the circuit only and can be found in [37].

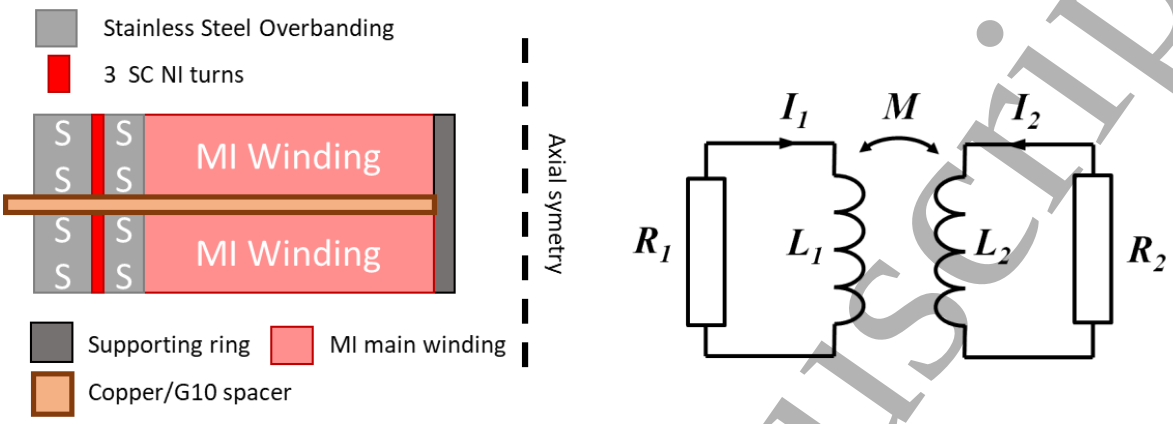

Figure 13: Magnetic shielding sketch (left) and simplified scheme of the electrical circuit of the HTS magnet (R1, L1, I1) and the magnetic shielding (R2, L2, I2) (right)

$$\begin{cases} i_1(t) = i_0\left(Ae^{-t/\theta_a} + Be^{-t/\theta_b}\right) \\ i_2(t) = Ci_0\left(e^{-t/\theta_a} - e^{-t/\theta_b}\right) \end{cases} \quad (2)$$

It is only very recently that we were able to evaluate completely the influence of the magnetic shield during NOUGAT fast transients. We developed our model based on a PEEC network, taking into account the redistribution of the currents both radially and azimuthally. We only consider a small magnet to evaluate the effect of this magnetic shielding because the computation for the whole NOUGAT insert is too time consuming. The small mock-up configuration consists of two doubles pancakes [13].

We performed a first simulation to understand the effect of the NI turns inside the overbanding. We modelled a four pancakes coil consisting of 200 MI turns for the main magnet and 10 NI turns inside the overbanding. We consider a convective cooling on inner and outer turns. The Table 3 summarizes the parameters.

Table 3: Small magnet and simulation parameter for NI Magnetic Shielding numerical study

Parameter	Unit	Value
Main magnet MI pancake turns	N/A	200
Outside NI turns	N/A	10
MI/NI Rct	μΩ.cm²	10000/70
MI/NI ID	mm	50/104.6

Cooling convection coefficient (h)	$W.m^{-2}.K^{-1}$	1000
Current (% LL)	A / %	107 / 10
Initial temperature	K	4.2

We present the simulation results in Figure 14. Each chart represents the four pancakes signals for the two cases (with or without magnetic shielding). At 3 ms we simulated the opening of the breaker and then the energy is discharged inside the winding (without MS) or shared between the winding and the magnetic shielding. We can identify the magnetic shielding effect on the azimuthal current decay (top right) which is much faster with a magnetic shielding. The effect is also visible on the maximum temperature reached by the magnet pancakes during the discharge. As a part of the stored energy is transferred and discharged in the NI turns, the main pancake peak temperatures reached with the NI magnetic shielding is lower than without. The central magnetic field decreases much faster at the beginning of the discharge, sign of the energy transfer to the NI turns. Then the magnetic shielding is dissipating the energy slowly through the NI turn-to-turn contact resistance (2-3 orders of magnitude lower than the MI winding). The SC magnetic shielding is therefore helping to lower quickly the azimuthal current at the onset of the discharge and avoid a too high local temperature. However, it also helps to avoid a too quick magnetic field decay, which might lead to a damage of the main winding because of unbalanced forces.

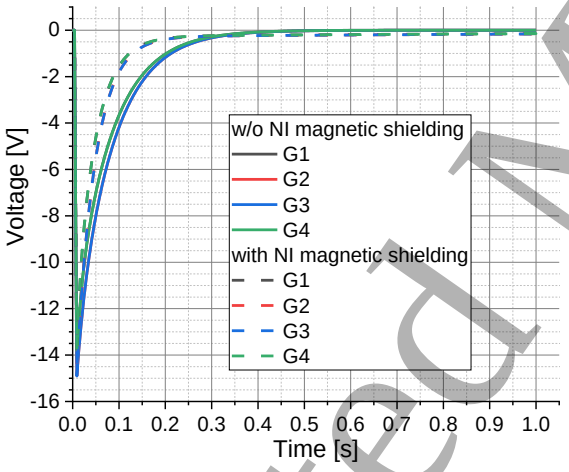

Pancake (w or w/o NI turns) turns voltages versus time

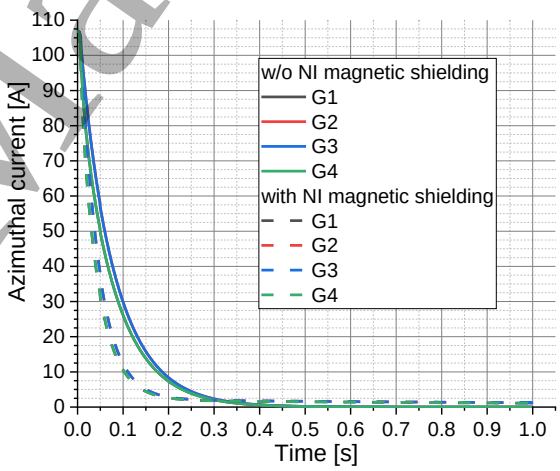

Azimuthal current (w and w/o NI turns) versus time

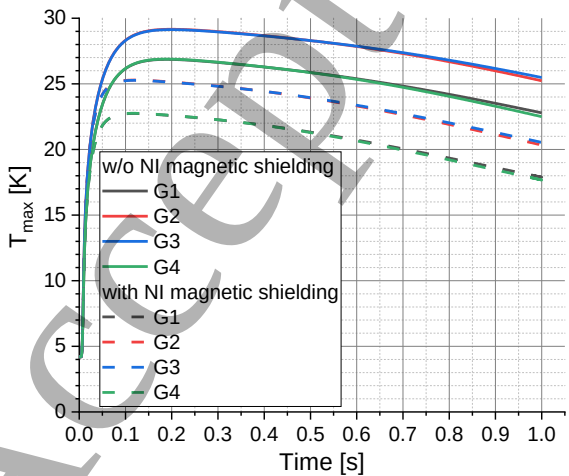

Maximum temperature of each pancake versus time

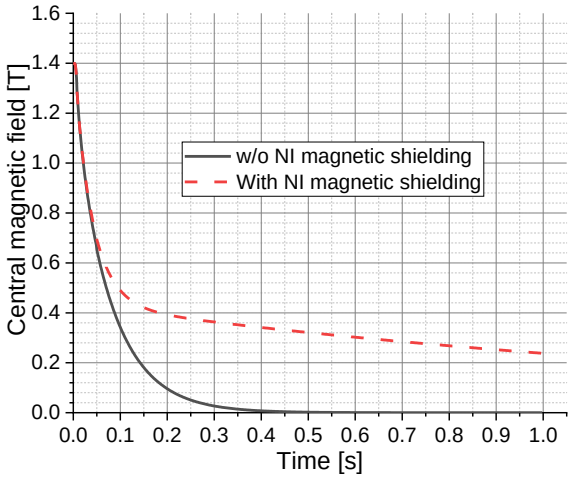

Field decay versus time: double constant due to NI turns

Figure 14: Numerical model of sudden discharge with and without magnetic shielding

VI. The protection of a MI magnet

In this section, we will discuss about the magnet protection or self-protection. In our meaning, a self-protected magnet means that nothing is done in the electrical circuit in order to actively or passively protect the magnet.

If the magnetic shielding plays an important role in the protection of the magnet by helping to lower the magnetic field fluctuation and then the induced voltages, currents and unbalance forces, it also helps to take out a part of the stored energy from the main winding. We might then look at what we can do to adapt a protection scheme to the magnet contact resistance range. By doing so, we should be able to determine the safe upper limit of the R_{ct}, and determine how to optimize the magnet protection. We consider that MI windings will not always present a self-protected feature, mostly for very high R_{ct} values. We therefore see this technology as a help during the onset of the resistive transition. With this help, we can let the voltage grows within the winding and then trigger an adapted protection scheme. As most of the quench occurs in a few hundreds of milliseconds, the protection with a dump resistor would require a too high voltage for high inductance magnets and the activation of heater would require a very high power in a not suitable delay due to the thermal stability of the winding [10].

We propose to use the high voltage generated by a quench in an MI coil for passively protecting the magnet at the beginning of the quench and then to trigger a protection to finish the magnet discharge. The idea is to consider the power supply as a voltage source when the coil is quenching. By adjusting the maximum allowable voltage (few hundreds of millivolts or few volts), we should be able to optimize the (R_{ct}/U_{max}) couple to protect effectively the magnet. We will present here some numerical results performed on a small pancake coil of 40 turns. We simulated the pancake behavior during transients using our PEEC model [9] [28], each turn being divided into 20 elements. We consider an adiabatic configuration in this simulation. We summarize the main parameters of the simulations in Table 4.

Table 4: MI protection numerical study parameters

Parameters	**unit**	**Value**
ID / OD	mm	50 / 55.6
Coil High	mm	6
Turns number	/	40
Sectors per turn / Total	/	20 / 800
Coil inductance	µH	142.05
Coil magnetic constant	mT/A	0.924
Initial temperature	K	4.2
Coil current (% Load Line)	A	657 (95%LL)
Time of quench ignition	ms	3
Simulation time step	ms	1
Simulation final time	s	< 1
R_{ct} range	µΩ.cm²	10^2-10^7
U_{max} range	V	0.005-10

All the simulations follow the same scheme: the coil is charged at 95 % on the load line at the beginning of the simulation. Then 3 ms later, we decrease by 50 % the critical current of one sector on turn 21.

We let the coil quench as the operating current exceeds the critical current in this sector. The simulation of the voltage limitation requires several iterations in order to adjust the coil current once U_{max} is reached. Such calculation are time consuming because of the loop to adjust the magnet current to the internal resistance and maximum voltage at each time step. To limit the computation time, we are looking at the coil current, which allows staying within in the range of 0.99-1 U_{max} (convergence criterion). We setup a timeout of the simulation at 1 second (considering that the interesting transient part is done at this time). Finally, we stopped the computation if the previous step current is fine to respect the convergence criterion. The main purpose of this numerical preliminary study is to evaluate the possibilities of protecting a magnet with a simple detection and passive protection scheme even at very high R_{ct} value.

We present the maximum hotspot temperature depending on the R_{ct} value and the maximum voltage in the 5 mV to 10 V range in Figure 15. For voltages up to 1 V, the hotspot temperature remains below 155 K, which is quite safe from the protection point of view even with very high R_{ct} of a few Ω.cm². If a maximum voltage of 5 mV is not representative of what can be applied on a real magnet (mainly because of signal noise inside a high inductance magnet), the 1 V limit seems to be acceptable and gives a remarkable illustration of the approach we proposed. The case of a voltage limit of 10 V shows the need of activating a protection (stop to power the coil) to avoid temperature above 200-250 K. Figure 16 and Figure 17 are presenting the simulation results for U_{max} = 1 V and U_{max} = 10 V respectively. We present the coil current, voltage, central magnetic field and maximum temperature for the two voltage limits. When considering 1 V as maximum voltage, all the winding with R_{ct} values up to 10 Ω.cm² seems self-protected, at least at the start of the quench. The coil current is automatically decreasing below 80 A for R_{ct} above 10 mΩ.cm², which leads to a reduced local heating power and hot spot temperature. The maximum temperature reached a pic and then remained relatively stable due to the thermal conduction inside the winding. This statement is valid in the duration of the simulation and we should confirm it on a longer time scale. When we consider the maximum voltage of 10 V, this protection method is less effective as the current is decreasing to a higher value and the local joule heating is therefore high. It generates a continuous increase of the local hotspot temperature, which might lead to the magnet damage if we do not trig a dedicated protection. Those two examples demonstrate that we have to consider a specific protection scheme for each solution. This technology is at least giving us the time for protecting a coil, even for very high turn-to-turn contact resistance. Figure 18 presents a zoom on the start of the quench after the local decrease of the SC performances at t= 3 ms. The coil voltage stays below 5 mV for about 400 ms before the quench occurs. It shows that the solution is locally protecting the conductor from a high hotspot spot temperature even when the R_{ct} value is above 1 Ω.cm². Once the voltage reaches about 10 mV, the magnet quench very quickly and if we do not protect the magnet or limit the voltage, the hotspot temperature increases above 250 K in less than 150 ms for high R_{ct} values. We performed the simulations on a small 40 turns pancake coil because of the computation time required. We planned to confirm all the statements presented in this section in the near future through simulation and experimental validation on multi-pancakes magnets with higher number of turns.

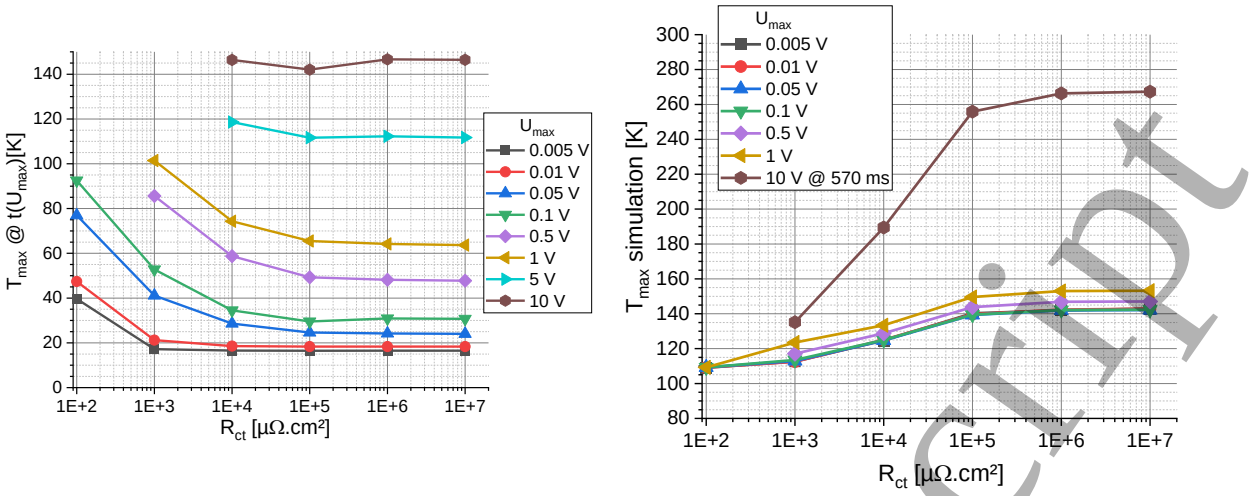

Figure 15: Maximum temperature reached depending on the R_{ct} value : when U_{max} is reached (left) and at 570 ms (right)

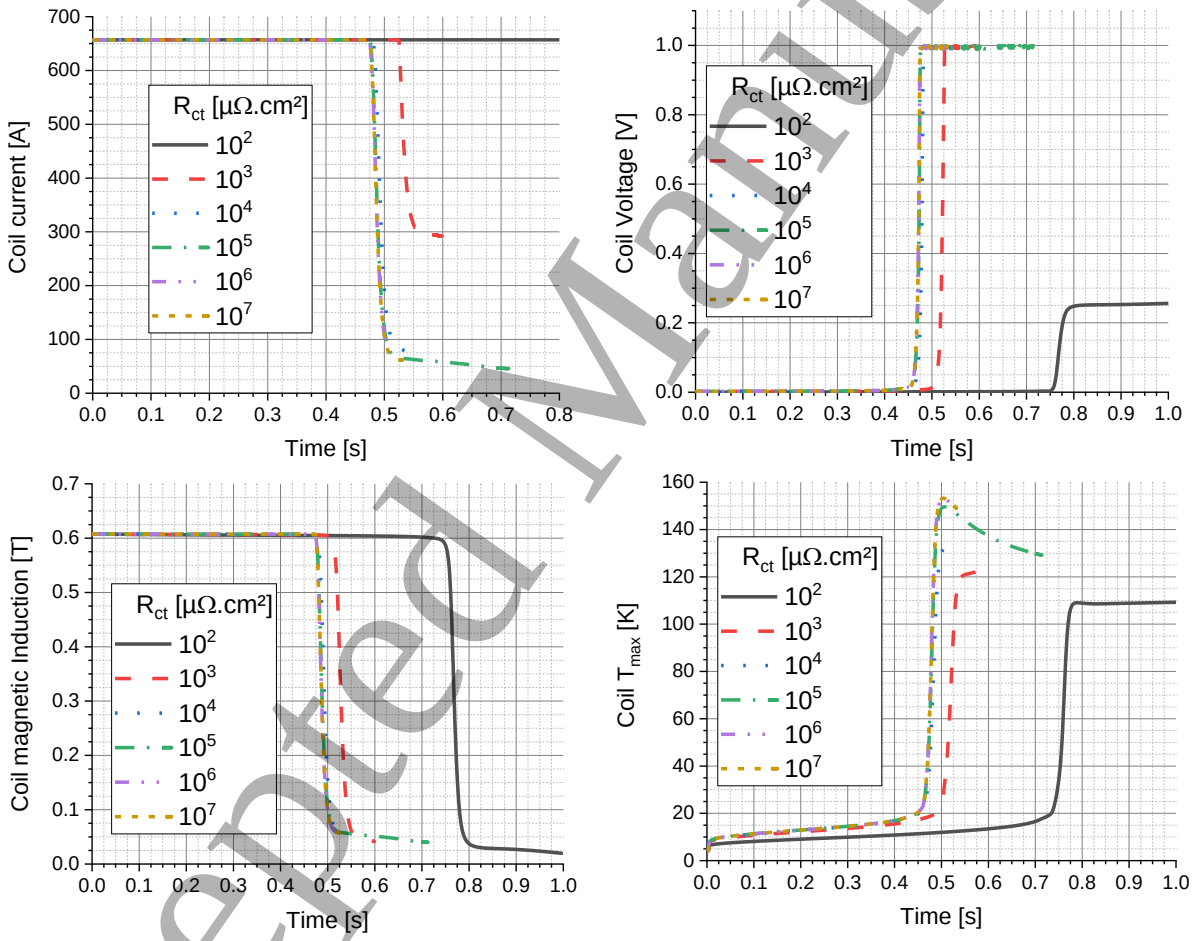

Figure 16: Example of U_{max} = 1 V

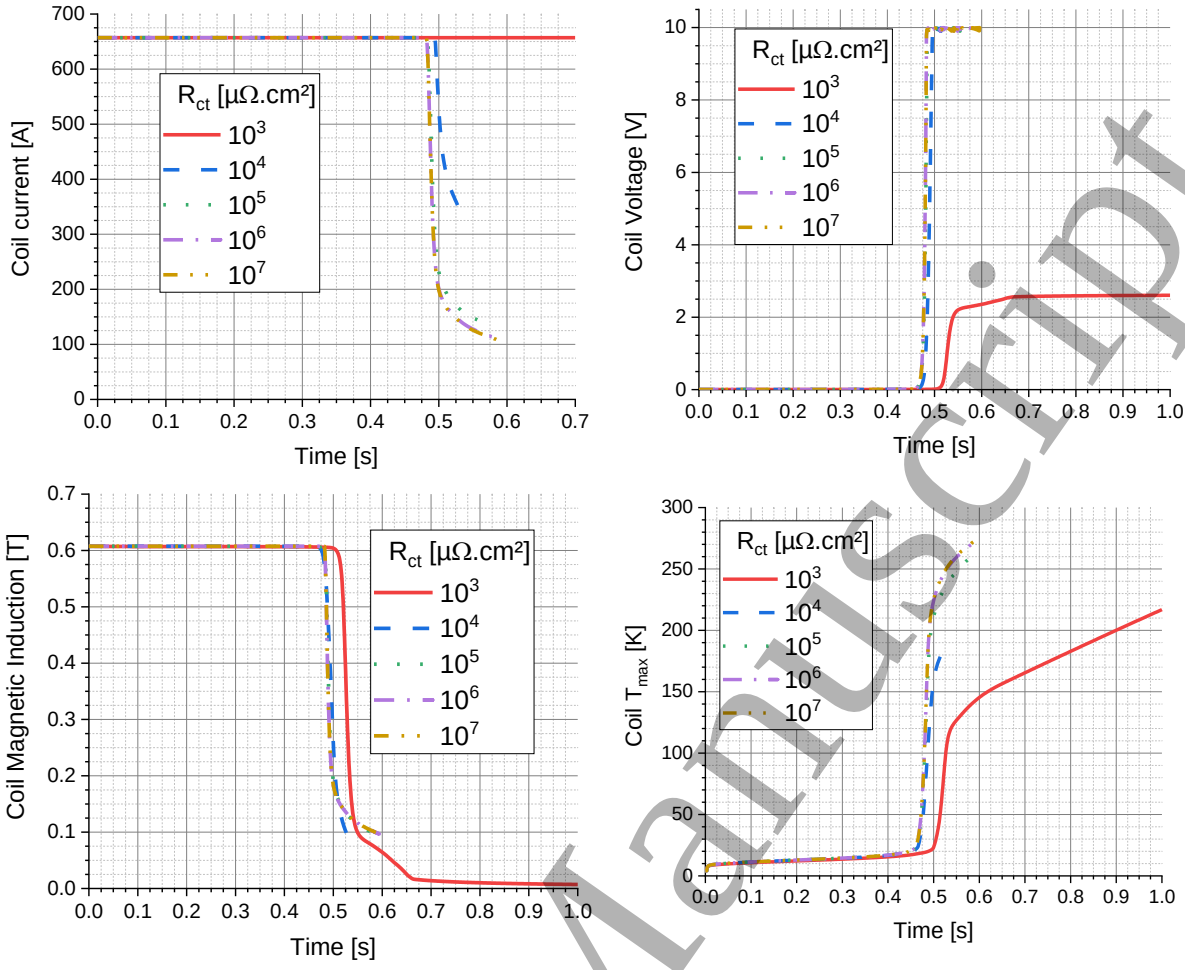

Figure 17: Example of U_{max}=10 V

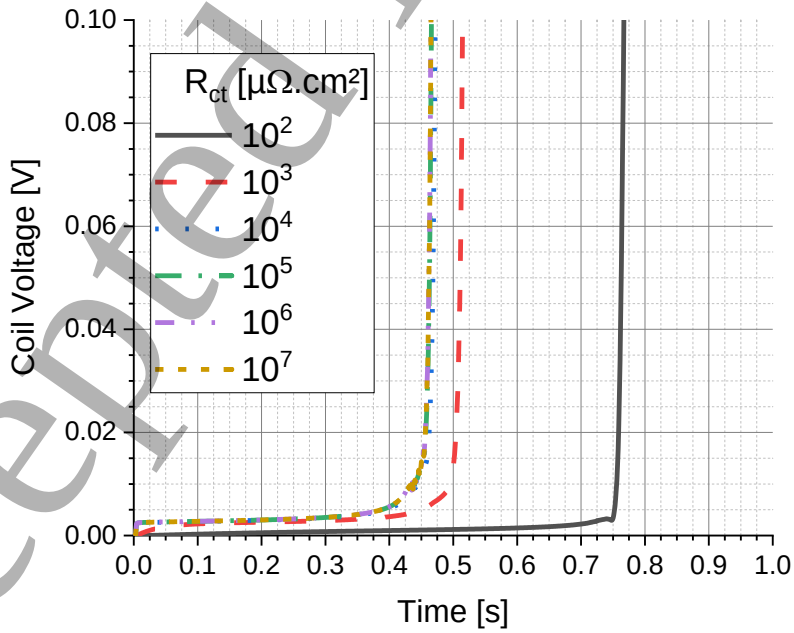

Figure 18 : 40 turns pancake voltage growth before quench

VII. Discussion: Avoiding local burning in the protection aspects

For the past ten years, research groups around the world have identified and widely developed a new approach for building HTS high field magnets. The main issue with HTS material and mainly with REBCO tape or cables remains the protection of the magnet in case of a local transition to the resistive state. The first idea was to find a way to improve the quench velocity by including a specific technology inside the HTS tapes in order to accelerate the propagation of the resistive zone, well know principle in LTS magnets. A practical way to process would be to include a current flow diverter architecture [38]. The technology is for now not available on a large-scale production.

The solution of removing the insulation for HTS magnet is a recent approach to design a magnet but also requires new tools for modelling and understanding in details the transient behavior. It is a very efficient approach, quite cheap and easy to develop in a first step. Nevertheless, the international community also highlighted new issues due to the generation of bypassing (radial) currents. They lead to unknown mechanical transient behavior, which might be critical for a magnet [39]. The MI technology, which we were the first to implement for protection aspects inside a high field magnet [12], is in fact a first step to the idea of tuning the contact resistance to the magnet purpose (fast or slow transients in normal operating conditions). The approach is to increase the resistance in order to lower the time constant and dissipations. Such winding presents the advantage of performing a nearly insulated behavior. It is also a simpler way for the winding process by avoiding smooth materials (e.g. the Kapton insulation) inside the winding. Going closer to the insulated magnet behavior in a MI magnet is also bringing the risk of coming back to the protection issue we had in the insulated HTS magnet. We detail below the question of the local burning and then discuss about what we might do to optimize the winding in terms of numerical approach and winding technologies.

The question of the protection is probably the more complex one. If we consider a classical approach of the protection, we need to be able to detect and discharge the stored energy (inside or outside the magnet) before a local high temperature hotspot is damaging the magnet. It implies to be able to see a very tinny signal in a noisy environment and to activate a protection scheme before the stored energy inside the magnet overheats a small part of the winding. The slower the propagation velocity, the harder the protection is. HTS magnets are designed with quite high operating margins to lower the risk of a local defect and burning. This operational (and so thermal) margin induces a relatively slow azimuthal propagation in an insulated HTS magnet, which is too slow to drive a significant part of a magnet above the critical temperature. It is why we have to increase the transited volume by heaters in UHF magnet with a high inductance [10]. The use of single HTS tapes or simple stack cables is for now the only option for UHF magnet developments in a reasonable time scale and budget, and with lower risks for the project. In a R_{ct} range, which still has to be defined, the radial currents in MI windings are abruptly lowering the field, and extra currents are induced in the highly magnetically coupled turns. Such extra currents are then quenching the turns much more quickly that the thermal propagation. For low values of R_{ct} the magnetic coupling will drive a full quench of a magnet in a very short time which is leading to a lower local hot spot temperature. It might be less efficient for high R_{ct} value for which the azimuthal currents are still high after a quench. Our experience on NOUGAT magnet quench at 32.5 T is that the whole HTS magnetic field has been discharged in about 700 ms without opening the beaker for driving a fast discharge inside the 1 Ω dump resistor. The magnet powering stopped as the magnet voltage went negative, which was not allowed by our one quadrant power supply. Despite the high R_{ct} of this winding type (in the 0.1-0.3 Ω.cm² range), the tests of our magnet confirmed that such technology is efficient to avoid any local high temperature hotspot inside the magnet. A simple OVP value set at a high tension compared to classical protection (0.5-1 V compared to a few tens of mV), or a power supply shut down once a significant part of the magnet is

already quenched, are efficient for protecting the magnet. With this solution, we do not need to open a breaker and discharge the current into a dump resistor, which might lead to a mechanical issue. In this configuration, the magnet energy is therefore discharge in the cryogenic environment, which boils off all the liquid helium inside the cryostat. We have now to determine the best protection scheme: opening a breaker or shutdown the power supply when a sufficient part of the magnet (to be determined) is already quenched. It is requested in order avoid continuing to dissipated power inside the cryogenics environment and eventually avoid to thermally damage the magnet (depending on the local cooling/joule heating ratio).

We proposed a protection approach in the part VI. The main consideration is that we have to adjust/choose the protection scheme depending on the magnet specificities. In particular, if we want a very short charging time constant, the magnet will require a high R_{ct} solution and therefore the hotspot temperature will increase in a critical mater. As the voltage increase inside a MI magnet is much faster than in a classical insulated HTS magnet, we can limit the Power Supply maximum voltage depending on the R_{ct} we have. By this way, we can significantly and passively decrease the current inside the magnet during the first tens or hundreds of milliseconds of the quench and then activate a protection consisting of discharging the remaining energy inside a dump resistor (use of a breaker) or inside the magnet (PS shutdown).

VIII. Conclusion

In this paper, we highlighted the aspects of the MI windings that we considered to be of great importance for a HTS user magnet. Our main message on this subject is that we need to consider such technology has a new one. Such assumption is leading to think again the protection scheme depending on the magnet type (required properties in terms of charging, stability and so on). We never will consider an MI magnet like self-protected, but we will consider that such windings might handle the onset of a quench without a complex detection and active protection. It allows the growth of the resistive volume and so the voltage development inside the magnet without any overheating risk. The choice we made for our UHF insert gave very promising results, showing that the protection of an MI HTS insert is still possible and easy even with a R_{ct} value in a few hundreds of $m\Omega.cm^2$. With so high values, the bypassing currents in the normal conditions are quite low and time constant reasonable. It seems to reduce the risk of critical unbalanced or torque forces, but this aspect has to be confirmed with specific models and experiments. The quite low bypassing currents might allow to use this technology in a wide range of magnets of high field applications. Nevertheless, the requested R_{ct} value might also be still too high for specific applications, which require a very high dB/dt and a good field quality during the ramping (like accelerator or gantry magnets).

Therefore, the R_{ct} is a key parameter and should be carefully adjust to the magnet requirements. Such optimization requires developing specific tools and technology:

1- A numerical toolbox for modelling a full magnet (electro-thermo-mechanical model) in a reasonable computation time. Although it is a big challenge, it will unlock the possibility of optimizing the resistance to the magnet type.
2- A practical way to measure and tune the resistance between turns and to limit its fluctuation in the space (between the turns inside one element and between the elements) and time (during the whole magnet lifetime).

In the section IV we gave a review of some R_{ct} values and technologies and highlighted a very important point: the R_{ct} values are depending on many parameters (from the materials and from the experimental set-up). Therefore, we have to choose a proper way to evaluated it, and look at all

parameters that might influence the value (tapes oxidation, mechanical/thermal cycling, pressure…). This is require in order to obtain the most accurate coil behavior evaluation from numerical studies.

Finally, the protection of MI windings can be completed by the adjustment of a technology proposed a few decades ago in order to implement and optimize a proper magnetic shielding. Adding some HTS NI turns inside the overbanding is an effective and promising way to implement this technology inside a compact HTS magnets. It also add another passive magnet protection. This solution presents the advantages of being very compact and very strong. The stainless steel overbanding is acting as a strong mechanical reinforcement, avoiding a mechanical failure of the magnetic shielding, and as a high enthalpy material for dissipating the energy.

IX. Acknowledgments

The authors acknowledge the support of the LNCMI-CNRS, member of the European Magnetic Field Laboratory (EMFL), and of the French National Research Agency (ANR) through the contracts ANR-10-LABX-51-01 (Labex LANEF – HTS winding project) and ANR-14-CE05-0005 (project NOUGAT, 'NOUvelle Génération d'Aimants pour la production de Teslas'). The analyzes were completed thanks to funding from the European Union's Horizon 2020 research and innovation program under grant agreement No 951714.

X. References

[1] R. E. Bailey, J. Burgeson, G. Magnuson and J. Parmer, "Metallic Insulation for Superconducting Coils". U.S. Patent Patent 4 760 365, 1988.

[2] R. Gupta, "High Field HTS R&D Solenoid for Muon Collider," *IEEE Trans. Appl. Supercond.,* vol. 21, no. 3, 2011.

[3] S. Hahn, D. K. Park, J. Bascuñán and Y. Iwasa, "HTS pancake coils without turn-to-turn insulation," *IEEE Trans. Appl. Supercond.,* vol. 21, no. 3, p. 1592–1595, 2011.

[4] P. Fazilleau, B. Borgnic, X. Chaud, . F. Debray, T. Lécrevisse and J.-B. Song, "Metal-as-insulation sub-scale prototype tests under a high background magnetic field," *Supercond. Sci. Technol.,* vol. 31, p. 095003, 2018.

[5] J. van Nugteren, *High Temperature Superconductor Accelerator Magnets,* 2016, pp. 64-65.

[6] J. Bascuñán, S. Hahn, D. K. Park and Y. Iwasa, "A 1.3-GHz LTS/HTS NMR Magnet- A Progress Report," *IEEE TRANSACTIONS ON APPLIED SUPERCONDUCTIVITY,* vol. 21, no. 3, 2011.

[7] X. Wang, S. Hahn, Y. Kim and J. Bascu˜n´an, "Turn-to-turn contact characteristics for equivalent circuit," *Supercond. Sci. Technol.,* vol. 26, p. 035012, 2013.

[8] T. Sung Lee, Y. J. Hwang, J. Lee, W. S. Lee, J. Kim, S. H. Song, M. C. Ahn and T. K. Ko, "The effects of co-wound Kapton, SS and copper, in comparison with no insulation, on the time constant and stability of GdBCO pancake coils," *Supercond. Sci. Technol.,* vol. 27, p. 065018, 2014.

[9] P. Fazilleau, T. Lecrevisse and X. Chaud, *Electrical behavior of Metal-as-Insulatin prototype coils for the ANR NOUGAT project,* Poster at Applied Superconductivity Conference (available upon request), 2016.

[10] H. V. Weijers, W. D. Markiewicz, A. V. Gavrilin, A. J. Voran, Y. L. Viouchkov and S. R. Gundlach, "Progress in the Development and Construction of a 32-T Superconducting Magnet," *IEEE Trans. Appl. Supercond.,* vol. 26, no. 4, pp. 1-7, 2016.

[11] S. Hahn, "Current Status of and Challenges for No-Insulation HTS Winding Technique," *J. Cryo. Super. Soc. Jpn.,* vol. 53, no. 1, 2018.

[12] P. Fazilleau, X. Chaud, F. Debray, T. Lécrevisse and J.-B. Song, "38 mm diameter cold bore metal-as-insulation HTS insert reached 32.5 T in a background magnetic field generated by resistive magnet," *Cryogenics,* p. 106, 2020. Cryogenics BEST PAPER AWARD 2020.

[13] J.-B. Song, C. Xavier, B. Benjamin, D. François, F. Philippe and L. Thibault, "Construction and Test of a 7 T Metal-as-Insulation HTS Insert Under a 20 T High Background Magnetic Field at 4.2 K," *IEEE Trans. Appl. Supercond.,* vol. 29, no. 5, 2019.

[14] K. Katsumata, T. Wang, A. Ishiyama, S. Noguchi, K. Monma, S. Nagaya and T. Watanabe, "Influence of the Turn-to-Turn Contact Electrical Resistance on the Thermal Stability in Meter-Class No-Insulation REBCO Pancake Coils During a Local Normal-State Transition," *IEEE Trans. Appl. Supercond.,* vol. 27, no. 4, pp. 1-5, 2017.

[15] J. Lu, J. Levitan, D. McRae and R. Walsh, "Contact resistance between two REBCO tapes the effects of cyclic loading and surface coating," *Supercond. Sci. Technol.,* vol. 31, p. 085006, 2018.

[16] S. Myung-Hwan, K. Sim, B. Eom, H.-S. Ha, H.-Y. Kim and K. Seong, "Controllability of the Contact Resistance of 2G HTS Coil With Metal Insulation," *IEEE TRANSACTIONS ON APPLIED SUPERCONDUCTIVITY,* vol. 28, no. 3, 2018.

[17] M. Bonura, C. Barth, A. Jourdrier, J. Ferradas Troitino, A. Fête and C. Senatore, "Systematic Study of the Contact Resistance Between REBCO Tapes: Pressure Dependence in the Case of No-Insulation, Metal Co-Winding and Metal-Insulation," *IEEE Trans. Appl. Supercond.,* vol. 29, no. 5, pp. 1-5, 2019.

[18] J. Vallier, "Annual report," GHMFL, Grenoble, France, 1996.

[19] P. Fazilleau, C. Berriaud, R. Berthier, F. Debray, B. Hervieu, W. Joss, F. P. Juster, M. Massinger, C. Mayri and Y. Queinec, "Final Design of the New Grenoble Hybrid Magnet," *IEEE Trans. Appl. Supercond.,* vol. 22, no. 3, p. 4300904–4300904., 2012.

[20] P. Fazilleau, G. Aubert, C. Berriaud, B. Hervieu and P. Pugnat, "Role and Impact of the Eddy Current Shield in the LNCMI-G Hybrid Magnet," *IEEE Trans. Appl. Supercond.,* vol. 26, no. 4, pp. 1-5, 2016.

[21] S. An, "A Feasibility Study on “Magnetic Dam” to Absorb Magnetic Energy in NI HTS Magnet During Quench," *IEEE Trans. Appl. Supercond.,* pp. VOL. 30, NO. 4, 2020.

[22] T. Mato, "Mechanical Damage Protection Method by Reducing Induced Current in NI REBCO Pancake Coils During Quench Propagation," *IEEE Trans. Appl. Supercond.,* 2021.

[23] W. D. Markiewicz, T. Painter, I. Dixon and M. Bird, "Quench transient current and quench propagation limit in pancake wound REBCO coils as a function of contact resistance, critical current, and coil size," *Superconductor Science and Technology,* vol. 32, no. 10, p. 14, 2019.

[24] T. Lécrevisse and Y. Iwasa, "A REBCO Pancake Winding With Metal As Insulation," *IEEE Trans. Appl. Supercond.,* vol. 26, no. 3, 2016.

[25] M.-H. Sohn, K. Sim, B. Eom, Y. W. Jeong, H.-S. Kim, D.-W. Ha and K. Seong, "Stability and quench behaviors of conduction-cooled 2G HTS Coil Cowound With SS Tape," *IEEE Trans. Appl. Supercond.,* vol. 26, no. 4, 2016.

[26] T. Lécrevisse, A. Badel, T. Benkel, X. Chaud, P. Fazilleau and P. Tixador, "Metal-as-insulation variant of no-insulation HTS winding technique pancake tests under high background magnetic field and high current at 4.2 K," *Supercond. Sci. Technol.,* vol. 31, p. 055008, 2018.

[27] J. Mun, C. Lee, K. Sim, C. Lee, M. Park and S. Kim, "Electrical Characteristics of Soldered Metal Insulation REBCO Coil," *IEEE Trans. Appl. Supercond.,* vol. 30, no. 4, 2020.

[28] C. Genot, T. Lécrevisse, P. Fazilleau and P. Tixador, *Transient behavior of a REBCO No-Insulation or Metal-as-Insulation multi-pancakes-or racetracks- coil using a Partial Element Equivalent Circuit model,* Magnet Technology 27, under review for publication in IEEE Transactions on Applied Superconductivity.

[29] J. Fleiter and A. Ballarino, "Parametrization of the critical surface of REBCO conductor from Fujikura," 2014.

[30] D. H. Kang, K. K. L., Y. G. Kim, Y. J. Park, W. J. Kim, S. H. Kim and H. G. Lee, "Investigation of thermal and electrical stabilities of a GdBCO coil using grease as an insulation material for practical superconducting applications," *Rev. Sci. Instrum.,* vol. 85, p. 094701, 2014.

[31] J. Kim, S. Yoon, K. Cheon, K. Hwan Shin and S. Hahn, "Effect of Resistive Metal Cladding of HTS Tape on the Characteristic of No-Insulation Coil," *IEEE Trans. Appl. Supercond.,* vol. 26, no. 4, 2016.

[32] D. G. Yang, Y. H. Choi, Y. G. Kim and J. B. Song, "Analytical and experimental investigation of electrical characteristics of a metallic insulation GdBCO coil," *Review of Scientific Instruments,* vol. 87, p. 034701, 2016.

[33] J. Lu, R. Goddard, K. Han and S. Hahn, "Contact resistance between two REBCO tapes under load and load cycles," *Supercond. Sci. Technol.,* vol. 30, p. 045005, 2017.

[34] M. Wang, Z. Li, J. Jiang, F. Dong, X. Xu, Z. Jin and K. Ryu, "Performance Study on the No-Insulation HTS Coil Wound With Narrow-Stacked Wire," *IEEE Trans. Appl. Supercond.,* vol. 30, 2020.

[35] J. Y. Jang, Y. Sangwon, H. Seungyong, H. Young Jin, K. Jaemin, S. Kang Hwan, C. Kyekun, K. Kwanglok, I. Sehwan, H. Yong-Ju, Y. Hankil, L. Hunju, M. Seung-Hyun and L. SangGap, "Design,

construction and 13 K conduction-cooled operation of a 3 T 100 mm stainless steel cladding all-REBCO magnet," *Supercond. Sci. Technol.,* vol. 30, p. 105012, 2017.

[36] S. Noguchi, "Turn-to-Turn Contact Resistance Measurement of No-Insulation REBCO Pancake Coils," *IEEE Trans. Appl. Supercond.,* vol. 29, no. 5, 2019.

[37] P. Fazilleau, F. Borgnolutti and T. Lécrevisse, "Protection Design for a 10-T HTS Insert Magnet," *IEEE Trans. Appl. Supercond.,* vol. 26, no. 3, 2016.

[38] C. Lacroix, Y. Lapierre, J. Coulombe and F. Sirois, "High normal zone propagation velocity in second generation high-temperature superconductor coated conductors with a current flow diverter architecture," *Supercond. Sci. Technol.,* vol. 27, p. 055013, 2014.

[39] D. Park, J. Bascu˜n´an, P. C. Michael, J. Lee, Y. H. Choi, Y. Li, S. Hahn and Iwasa, "MIT 1.3-GHz LTS/HTS NMR Magnet: Post Quench Analysis and New 800-MHz Insert Design," *IEEE Trans. Appl. Supercond.,* vol. 29, no. 5, pp. 1-4, 2019.